J Electr Eng Technol Vol. 8, No. 4: 719-728, 2013
http://dx.doi.org/10.5370/JEET.2013.8.4.719

ISSN(Print) 1975-0102
ISSN(Online) 2093-7423

# Probabilistic Assessment of Voltage Stability Margin in Presence of Wind Speed Correlation

**Hongxin Li†, DeFu Cai* and Yinhong Li***

**Abstract** – Probabilistic assessment of voltage stability margin (*VSM*) with existence of correlated wind speeds is investigated. Nataf transformation is adopted to establish wind speed correlation (WSC) model. Based on the saddle-node bifurcation transversality condition equations and Monte Carlo simulation technique, probability distribution of *VSM* is determined. With correlation coefficients range low to high value, the effect of WSC on *VSM* is studied. In addition, two risk indexes are proposed and the possible threat caused by WSC is evaluated from the viewpoint of risk analysis. Experimental results show that the presence of correlated wind speeds is harmful to safe and stable operation of a power system as far as voltage stability is concerned. The achievement of this paper gives a detailed elaboration about the influence of WSC on voltage stability and provides a potentially effective analytical tool for modern power system with large-scale wind power sources integration.

**Keywords**: Voltage stability, Saddle-node bifurcation, Wind power, Wind speed correlation, Nataf transformation, Monte carlo simulation

## 1. Introduction

Voltage stability investigation is an important branch of power system stability researches and to prevent voltage collapse is a crucial prerequisite for electrical power network safety and reliability [1]. With the aggravation of energy crisis across the world, renewable energy power source such as wind power has been increasingly brought into power grid. Due to the uncertainty of wind speed, wind farm output generally shows strong stochastic property. Probabilistic voltage stability assessment with consideration of wind power stochastic property is a valuable topic in current power system [2].

Wind farms with close locations are usually in the same geographically wind belt, where wind speeds of these wind farms have strong correlation relationship. Therefore power generations of adjacent wind farms are spatially correlated [3]. When a power system is integrated with multiple close located wind farms, wind speed correlation (WSC) will strengthen the synchronization of different wind farm's power generation, and consequently increase the fluctuation of total wind power. With constant promotion of wind power in modern power grid, the impact of WSC on planning and operation should be carefully studied [4].

The effect of WSC on power system has been investigated in several technical literatures, and the researches focus on various aspects such as probabilistic power flow (PPF) [5-8], reliability evaluation [9-11], adequacy assessment [12-13], small-signal stability analysis [14] and economic dispatch [15]. In [5], a PPF technique based on extended point estimate method and orthogonal transformation is proposed. Reference [5] concludes that the expected values of output variables remain basically unchanged as the correlation among input random variables increases, however, the standard deviations of output variables increase significantly as the correlation grows. In [9], a Monte Carlo (MC) simulation based reliability evaluation procedure considering WSC is developed. The indices loss of load expectation (LOLE) and loss of energy expectation (LOEE) increase as the correlation degree increases. Based on state sampling MC simulation technique, reference [12] investigates the contributions of large-scale wind farms with different degrees of WSC to the load point and system reliability indices. In [14], a probabilistic small-signal stability analysis method is proposed. Spatial correlation of adjacent wind farms is considered by cross cumulant technique and test results indicate that the consideration of WSC has changed probabilistic density function curve of the real part of critical eigenvalue. In [15], a novel economic dispatch formulation that takes into account both correlated wind speeds and autocorrelation for each location is put forward. Results of the case study reveal that a more expensive generation cost is given when correlation is included.

Despite above recent works, however, the impact of WSC on power system voltage stability is seldom analyzed specially. The insufficient research in this field motivates the work reported in this paper, where voltage stability evaluation with consideration of wind speed correlation and

† Corresponding Author: The State Key Laboratory of Advanced Electromagnetic Engineering and Technology, Huazhong University of Science and Technology, China. (lihongxin0308@gmail.com)
* The State Key Laboratory of Advanced Electromagnetic Engineering and Technology, Huazhong University of Science and Technology, China.
Received: July 26, 2012; Accepted: March 5, 2013

wind farm output stochastic property is comprehensively studied. The main contributions of this paper are three-fold:

1. Nataf transformation is incorporated into voltage stability evaluation using Monte Carlo simulation technique. The results demonstrate the differences in voltage stability margin (*VSM*) probability distribution under varied wind speed correlation coefficients.
2. Two risk indexes for voltage stability evaluation with consideration of WSC are presented. The possible threat to *VSM* caused by WSC is evaluated from the viewpoint of risk analysis.
3. Impact of wind power penetration level as well as wind turbine's power factor on *VSM* is also investigated. Positive and negative influences are discussed.

The rest of the paper is organized as follows. In Section 2, Nataf transformation is summarized and adopted to establish the WSC model. Section 3 gives the wind farm model. Procedure of *VSM* probabilistic assessment considering correlated wind speeds is proposed in Section 4. Two risk indexes for voltage stability evaluation are presented in Section 5. Case study is provided in Section 6. Finally, the paper concludes in Section 7.

## 2. Wind Speed Correlation Modeling

In this paper, Nataf transformation is adopted to establish wind speed correlation model. The correlated wind speed vector can be transformed to independent standard normal variable vector with implementation of Nataf transformation, and the random samples of correlated wind speeds are generated by inverse Nataf transformation [16].

### 2.1 Nataf transformation

Nataf transformation is a mathematical model for the transformation from correlated original space to mutually independent standard normal one. It requires the marginal cumulative distribution function (CDF) of each random variable and their correlation coefficient matrix (CCM), which are easy to be obtained in engineering applications [17-18].

When the marginal CDF $\boldsymbol{F}(\boldsymbol{V}) = [F_1(v_1),\ F_2(v_2), \ldots, F_n(v_n)]^T$ and the CCM $\boldsymbol{\rho}_V$ of correlated wind speed vector $\boldsymbol{V}=[v_1,v_2,\ldots,v_n]^T$ are available, a correlated standard normal variable (SNV) vector $\boldsymbol{Y}= [y_1, y_2, ..., y_n]^T$ can be obtained by marginal transformation [19]

$$y_i = \Phi^{-1}(F_i(v_i)) \quad i = 1,2,...,n \tag{1}$$

where $\Phi(\bullet)$ is the CDF of SNV.

Denote $\boldsymbol{\rho}_Y$ as the CCM of vector $\boldsymbol{Y}$, the relationship between correlation coefficient $\rho_{vij}$ and $\rho_{yij}$ can be expressed as [20]

$$\rho_{vij} = \int_{-\infty}^{+\infty}\int_{-\infty}^{+\infty} \left(\frac{F_i^{-1}(\Phi(y_i)) - \mu_i}{\sigma_i}\right)\left(\frac{F_j^{-1}(\Phi(y_j)) - \mu_j}{\sigma_j}\right) \varphi_2(y_i, y_j, \rho_{yij}) dy_i dy_j \tag{2}$$

where $\rho_{vij}$ and $\rho_{yij}$ are elements of CCM $\boldsymbol{\rho}_V$ and $\boldsymbol{\rho}_Y$, $\mu_i$ and $\sigma_i$ are, respectively, the mean and standard deviation (SD) of wind speed $v_i$; $\varphi_2(y_i, y_j, \rho_{yij})$ is the two-dimensional standard normal probability density function of zero means, unit SD, and correlation coefficient $\rho_{yij}$.

To avoid complex integral operation, Liu and Der Kiureghian presented the empirical formula to approximately determine the solution of (2) for Weibull distribution as follows [19]

$$\rho_{yij} = D(\rho_{vij})\rho_{vij} \tag{3}$$

where

$$D(\rho_{vij}) = 1.063 - 0.004\rho_{vij} - 0.2\left(\frac{\sigma_i}{\mu_i} + \frac{\sigma_j}{\mu_j}\right) - 0.001\rho_{vij}^2 + 0.337\left(\left(\frac{\sigma_i}{\mu_i}\right)^2 + \left(\frac{\sigma_j}{\mu_j}\right)^2\right) + 0.007\rho_{vij}\left(\frac{\sigma_i}{\mu_i} + \frac{\sigma_j}{\mu_j}\right) - 0.007\left(\frac{\sigma_i}{\mu_i}\right)\left(\frac{\sigma_j}{\mu_j}\right)$$

For given $\boldsymbol{F}(\boldsymbol{V})$ and $\boldsymbol{\rho}_V$, $\boldsymbol{\rho}_Y$ can be computed by (3). In most engineering applications, $\boldsymbol{\rho}_Y$ is positive definite. So it can be decomposed by Cholesky decomposition

$$\boldsymbol{\rho}_Y = \boldsymbol{G}_Y \boldsymbol{G}_Y^T \tag{4}$$

where $\boldsymbol{G}_Y$ is an inferior triangular matrix. Based on $\boldsymbol{G}_Y$, the correlated SNV vector $\boldsymbol{Y}$ can be transformed into a new vector $\boldsymbol{X}=[x_1,x_2,\ldots,x_n]^T$ of independent standard normal variables in the following manner.

$$\boldsymbol{X} = \boldsymbol{G}_Y^{-1}\boldsymbol{Y} \tag{5}$$

Performing (1)~(5) transforms correlated wind speed vector $\boldsymbol{V}$ to independent SNV vector $\boldsymbol{X}$ .These procedures are the positive process of Nataf transformation.

### 2.2 Generation of correlated wind speed samples

The random samples of correlated wind speeds can be generated by inverse Nataf transformation when $\boldsymbol{F}(\boldsymbol{V})$ and $\boldsymbol{\rho}_V$ are available. The main steps are as follows.

1) Generate random samples $\boldsymbol{X}_s$ of independent SNV vector $\boldsymbol{X}$.
2) Obtain the CCM $\rho_Y$ of correlated SNV vector $Y$ by (3).

Decompose this matrix by Cholesky decomposi-tion and get $G_Y$.

3) Generate random samples $\boldsymbol{Y}_s$ of vector $\boldsymbol{Y}$ by (6).

$$\boldsymbol{Y}_s = \boldsymbol{G}_Y \boldsymbol{X}_s \tag{6}$$

4) Generate correlated random samples $\boldsymbol{V}_s$ of wind speed vector $\boldsymbol{V}$ by marginal transformation as (7).

$$\boldsymbol{V}_s = \boldsymbol{F}^{-1}(\boldsymbol{\Phi}(\boldsymbol{Y}_s)) \tag{7}$$

## 3. Wind Farm Modeling

A wind farm that can produce bulk active power is established by installing and utilizing many wind turbines. Power output of a wind farm depends on the power generation of wind turbines in the farm, while the working efficiency of a wind turbine is determined by wind speed. Wind farm model is developed by knowing wind speed probability distribution and wind turbine model.

### 3.1 Probability distribution of wind speed

Several previous works have investigated wind speed statistical characteristics and presented lot kinds of probability distributions to evaluate wind speed, such as Weibull, Rayleigh and LogNormal [21-22]. A Weibull distribution, which the wind speed profile at a given location most closely follows over time [23], is taken in this paper. The probability density function for a Weibull distribution is given by

$$f(v) = \frac{k}{c}\left(\frac{v}{c}\right)^{k-1} \exp[-\left(\frac{v}{c}\right)^{k}] \tag{8}$$

where $v$ denotes wind speed; $k$ and $c$ are scale parameter and shape parameter respectively.

### 3.2 Wind turbine model

Power output of a wind turbine is related to wind speed and there is a nonlinear relationship between them. It is assumed that all wind farms are equipped with IEC IIA wind turbine in this paper. Active power output of the IEC IIA wind turbine $P_{WT}$ with a given wind speed input $v$ may be stated as [24]

$$P_{WT}(v) = \begin{cases} 0 & v < v_{ci} \\ P_r \dfrac{v^2 - v_{ci}^2}{v_r^2 - v_{ci}^2} & v_{ci} \le v < v_r \\ P_r & v_r \le v < v_{co} \\ 0 & v \ge v_{co} \end{cases} \tag{9}$$

where $P_r$ is the rated power of the wind turbine; $v_{ci}$, $v_r$ and $v_{co}$ are respectively cut-in, rated and cut-out speed of the wind turbine.

### 3.3 Wind farm output

Denote $NT_i$ as the number of wind turbines installed in the wind farm connected to bus $i$. Active power output of the wind farm located at bus $i$, i.e. $P_{WF,i}$ is the sum of active power generation of wind turbines included in it, as

$$P_{WF,i} = \sum_{j=1}^{NT_i} P_{WT,j} \tag{10}$$

where $P_{WT,j}$ is active power generation of the $j^{th}$ wind turbine in the wind farm.

Reactive power consumption of a wind farm depends on the wind turbine type and the operation mode. In practice, recent grid codes of many countries require that grid-connected wind farms should provide reactive power control capabilities and network operators may specify power factor requirement for the wind farms [25]. Thus, for a given wind farm, $PQ$ model with constant power factor is adopted in this paper and the reactive power consumption $Q_{WF,i}$ can be computed as

$$Q_{WF,i} = P_{WF,i} \cdot \tan\theta_i \tag{11}$$

where $\theta_i$ is the power factor angle of wind turbines installed in the wind farm connected to bus $i$.

## 4. Probabilistic Assessment of Voltage Stability Margin

### 4.1 Voltage stability margin: problem formulation and calculation method

*VSM* indicates the precise distance between current operating state and voltage collapse critical state for a given system, which is an effective index used to evaluate voltage stability in academic research as well as engineering practice.

Fig. 1 shows the well-known PV-curve, which can be obtained by continuation methods [26]. The horizontal axis $P$ represents total active power load of a given system, and the vertical axis $V_i$ denotes voltage magnitude for a certain bus $i$. As the system load increases, voltage level declines, the lower branch of PV-curve beyond the nose point is corresponding to unstable region where bus voltage is uncontrollable. The allowable system active power load increment from current operating state to the critical state (nose point in Fig. 1) is defined as *VSM*.

Voltage stability critical state is related to saddle-node bifurcation (SNB) of the power flow equations [27]. The following transversality conditions can be used to

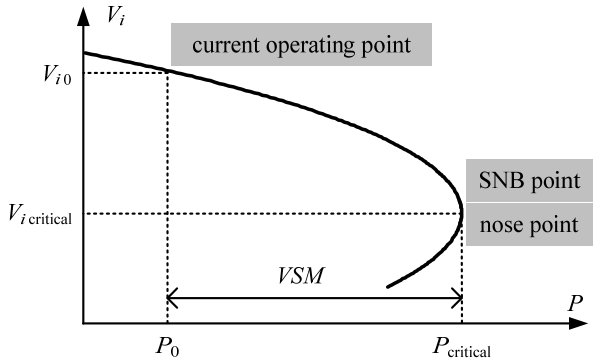


**Fig. 1.** Graphic representation of PV-curve and *VSM*

characterize and detect SNB [28-29]

$$\boldsymbol{f}(\boldsymbol{x},\lambda)=0 \tag{12}$$

$$\boldsymbol{f}_x(\boldsymbol{x},\lambda)\cdot\boldsymbol{v}=0 \tag{13}$$

$$\boldsymbol{l}^T\cdot\boldsymbol{v}-1=0 \tag{14}$$

where $\boldsymbol{f}(\boldsymbol{x}, \lambda)$ in (12) is the extended power flow equations which can be detailed as (15) and (16); $\lambda$ is a scalar bifurcation parameter and is known as the "loading factor"; $\boldsymbol{x} = [\boldsymbol{\theta}, \boldsymbol{V}]^{\mathrm{T}}$ is a vector of state variables which represent *PQ* bus voltage angles $\boldsymbol{\theta}$ and voltage magnitudes $\boldsymbol{V}$. The SNB characteristic equations in (13) implies that $\boldsymbol{f}_x(\boldsymbol{x}, \lambda)$, i.e. the Jocabian matrix of power flow equations is singular; $\boldsymbol{v}$ is a vector of normalized right eigenvectors. The normalized function expressed by (14) is used to restrain $\boldsymbol{v}$ not equal to zero. Generally, $\boldsymbol{l}$ is set to $\boldsymbol{e}_p$, a vector has same dimension with $\boldsymbol{v}$. In $\boldsymbol{e}_p$ the $p^{\text{th}}$ element is equal to one while other elements are all zero.

The incompact expression of the extended power flow equations $\boldsymbol{f}(\boldsymbol{x}, \lambda)$ is as follows.

$$\begin{aligned}\Delta P_i &= P_{Gi}(\lambda)+P_{\mathrm{WF},i}-P_{Li}(\lambda)\\ &-V_i\sum_{j=1}^{N}V_j[G_{ij}\cos\theta_{ij}+B_{ij}\sin\theta_{ij}]=0, i\in N_{PV},N_{PQ}\end{aligned} \tag{15}$$

$$\begin{aligned}\Delta Q_i &= Q_{cri}-Q_{\mathrm{WF},i}-Q_{Li}(\lambda)\\ &-V_i\sum_{j=1}^{N}V_j[G_{ij}\sin\theta_{ij}-B_{ij}\cos\theta_{ij}]=0,\ i\in N_{PQ}\end{aligned} \tag{16}$$

where $P_{Gi}(\lambda)$ denotes active power generation of conventional generator at bus *i*; $P_{\mathrm{WF}i}$ and $Q_{\mathrm{WF}i}$ respectively represent active power generation and reactive power consumption of wind farm at bus *i*. Active and reactive power load at bus *i* are expressed as $P_{Li}(\lambda)$ and $Q_{Li}(\lambda)$. $Q_{cri}$ is the reactive compensation capacity at bus *i*. $V_i$ is the voltage magnitude at bus *i*; $\theta_{ij}$ is the voltage phase angles difference between bus *i* and bus *j*. $G_{ij}$ and $B_{ij}$ denote the transfer conductance and susceptance between bus *i* and bus *j* respectively. *N* is the number of buses; $N_{PV}$ and $N_{PQ}$ are the set of *PV* buses and *PQ* buses. $P_{Gi}(\lambda)$, $P_{Li}(\lambda)$ and $Q_{Li}(\lambda)$ are all functions of bifurcation parameter $\lambda$, their concrete forms are dependent on the load increasing pattern and the mode of power dispatch among generators. The detail model of $P_{Gi}(\lambda)$, $P_{Li}(\lambda)$ and $Q_{Li}(\lambda)$ adopted in this work is illustrated in case study.

The transversality conditions expressed by (12)~(14) are nonlinear equations. For solving these equations and obtaining $\boldsymbol{x}$, $\boldsymbol{v}$, and $\lambda$ corresponding to voltage collapse critical state, the linearized equations as (17) is established and Newton–Raphson method can be utilized to iterative calculation.

$$\begin{bmatrix}\boldsymbol{f}_x & 0 & \boldsymbol{f}_\lambda\\ \boldsymbol{f}_{xx}\cdot\boldsymbol{v} & \boldsymbol{f}_x & 0\\ 0 & \boldsymbol{e}_p^T & 0\end{bmatrix}\begin{bmatrix}\Delta\boldsymbol{x}\\ \Delta\boldsymbol{v}\\ \Delta\lambda\end{bmatrix}=-\begin{bmatrix}\boldsymbol{f}(\boldsymbol{x},\lambda)\\ \boldsymbol{f}_x\cdot\boldsymbol{v}\\ 0\end{bmatrix} \tag{17}$$

In (17), $\boldsymbol{f}_\lambda$ is partial derivatives matrix for the ratio between $\boldsymbol{f}(\boldsymbol{x}, \lambda)$ and $\lambda$; $\boldsymbol{f}_{xx}$ is the Hessian matrix of power flow equations. $\Delta\boldsymbol{x}$, $\Delta\boldsymbol{v}$ and $\Delta\lambda$ represent increment of $\boldsymbol{x}$, $\boldsymbol{v}$, and $\lambda$ respectively.

In order to reduce computational efforts of the high dimensional Newton iterative equations, matrix reduction technique presented in [30] is adopted to solve (17) and $\boldsymbol{x}$, $\boldsymbol{v}$, and $\lambda$ are obtained. Based on $\lambda$, active power demand at load buses corresponding to the voltage collapse critical state, i.e. $P_{Li}(\lambda)$ can be determined. Voltage stability margin is finally calculated as follows.

$$VSM=\sum_{i=1}^{N}P_{Li}(\lambda)-\sum_{i=1}^{N}P_{Li,0} \tag{18}$$

where $P_{Li0}$ stands for base active load level of bus *i* in the initial operating state.

### 4.2 Probabilistic *VSM* assessment based on Monte Carlo simulation

In the mathematical model (12)~(14) for power system *VSM* determination, correlation of wind speeds and probabilistic behavior of wind farm outputs are considered, and a probabilistic *VSM* assessment model can be established. The input random variable of the probabilistic assessment model is $\boldsymbol{V}=[v_1, v_2,\ldots, v_n]^T$, i.e. vector of correlated wind speeds of wind farms, while the response is voltage stability margin.

For given marginal CDF $\boldsymbol{F}(\boldsymbol{V})$ and CCM $\boldsymbol{\rho}_V$ of correlated wind speed vector $\boldsymbol{V}$, different wind samples are produced by Monte Carlo simulation and *VSM* is computed with implementation of (17) and (18). The general procedure of probabilistic *VSM* assessment is as follows.

1) Input the data of a electric power system and configure the number of Monte Carlo simulation samples as *NS*.
2) Based on $\boldsymbol{F}(\boldsymbol{V})$ and $\boldsymbol{\rho}_V$, perform Nataf transformation

and generate *NS* samples, each of which is a correlated random wind speed vector $\boldsymbol{V}_s$ satisfying a certain correlation coefficient matrix.

3) Set $k = 1$.
4) For $\boldsymbol{V}_s=[v_1,v_2,\ldots,v_n]^T$ in the $k^{th}$ sample, active power generation $P_{WFi}$ and reactive power consumption $Q_{WFi}$ of the wind farm connected to bus $i$ are calculated by (9)~(11).
5) The calculation for linearized Eqs. (17) is implemented, with extended power flow Eqs. (15, 16) adopted and wind farm power $P_{WFi}$ as well as $Q_{WFi}$ considered.
6) Determine *VSM* corresponding to the $k^{th}$ Monte Carlo sample by (18).
7) Check whether the maximum Monte Carlo simulation limit *NS* is reached. If not, $k = k+1$ and go to step 4).
8) Depict statistical histogram of voltage stability margins for multiple samples, and the *VSM* probability distribution under a certain wind speed correlation degree is obtained.

## 5. Risk Analysis

Probabilistic assessment methods provide a range of *VSM* values with their probabilities instead of a deterministic value. With respect to probabilistic variation of *VSM*, a desired *VSM* value is associated with a certain risk. In this paper, two risk evaluation indexes similar with probabilistic assessment of Total Transfer Capability in [31] are presented.

1) In the operation of a given electric power network, it is a customary expectation that generation and transmission system can support more power load growth, thus the high value of voltage stability margin is desired. From this point of view, having any *VSM* values lower than a given $VSM_S$ is considered as risk. So risk of not achieving a specific $VSM_S$ is equal to the probability that voltage stability margin is less than or equal to $VSM_S$ as follows.

$$Risk_1(VSM_s) = \frac{N(VSM \le VSM_s)}{NS} \times 100\% \qquad (19)$$

where $N(VSM \le VSM_S)$ is the number of Monte Carlo simulation samples in which obtained *VSM* values are equal to or less than $VSM_S$.

2) In addition to considering the probability of having *VSM* values lower than a specific $VSM_S$, for each Monte Carlo sample satisfying $VSM \le VSM_S$, the amount of voltage stability margin deficiency, i.e. $(VSM_S - VSM)$ is also considered. The second risk index indicates the summation of standardized margin shortages corresponding to $VSM_S$ and can be formulated as

$$Risk_2(VSM_s) = \frac{1}{NS} \cdot \sum_{VSM \le VSM_s} \frac{VSM_s - VSM}{VSM_s} \times 100\% \qquad (20)$$

The index $Risk_2$ denotes cumulative effect of margin deficiencies and provides a novel perspective for evaluating risk degree of voltage instability.

According to the above two risk index values, network operators may perform more sophisticated analysis and judgment about *VSM* with large-scale wind power penetration. This information is helpful to determine or modify operation protocols and control strategies which are beneficial to the enhancement of voltage stability.

## 6. Case Study

### 6.1 Test system and parameter settings

To investigate the effect of WSC on *VSM*, a modified IEEE 57-bus system with four grid-connected wind farms is used as the test system, which is shown in Fig. 2.

Since the selection of installing locations of wind generators is not the issue of discussion in this paper, it is assumed that the wind farms have already been established at bus 4, 5, 54 and 55. This assumption does not affect the investigation as well as test of the presented probabilistic assessment methods. WSC is closely related to the

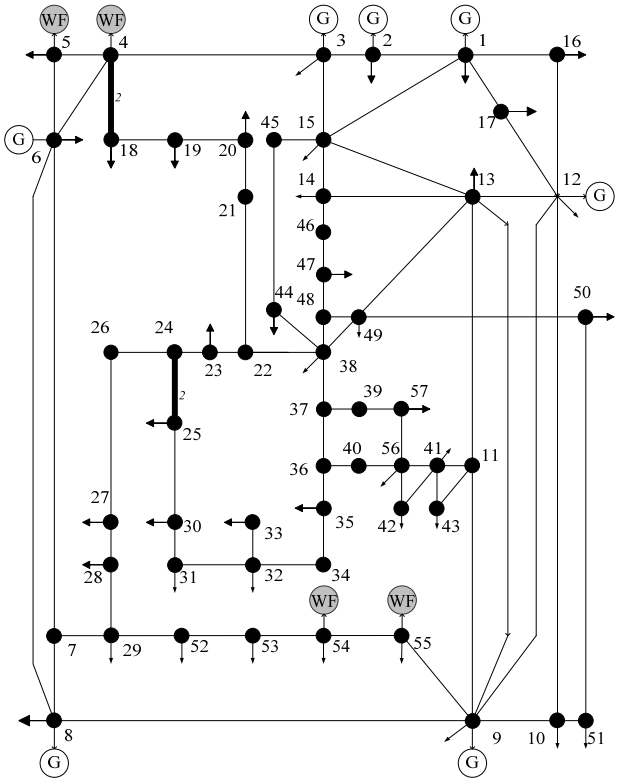


**Fig. 2.** Modified IEEE 57-bus system integrated with four wind farms

geographical distance between wind farms. It is a reasonable assumption that wind speed at bus 4 is correlated in certain degree with wind speed at bus 5, because of their close locations. Similarly, it is assumed that wind speeds at bus 54 and bus 55 have correlation relationship to some extent. WSC between bus $i$ and bus $j$ can be expressed by their correlation coefficient $\rho_{Vi,j}$ and the following CCM $\boldsymbol{\rho}_V$ is established for four grid-connected wind farms.

$$\boldsymbol{\rho}_V = \begin{bmatrix} 1 & \rho_{V4,5} & 0 & 0 \\ \rho_{V5,4} & 1 & 0 & 0 \\ 0 & 0 & 1 & \rho_{V54,55} \\ 0 & 0 & \rho_{V55,54} & 1 \end{bmatrix} \tag{21}$$

Total installation capacity of the four grid-connected wind farms is 256 MW, which is approximately 20% of active power load in initial operating state of IEEE 57-bus system. The installed capacity is equally divided into four wind farms. Each wind farm includes 32 IEC IIA wind turbines. Table 1 summarizes main parameters of IEC IIA wind turbine [24]. The same Weibull distribution with scale parameter $k$ and shape parameter $c$ equal to 9.1 and 2.7 respectively is used to model wind speed at four different buses. Sample size of Monte Carlo simulation is set to 10000. Wind speed samples with given CCM $\boldsymbol{\rho}_V$ is obtained from inverse Nataf transformation mentioned in section 2.2, and wind farm power output is calculated with implementation of (9)~(11). The load increasing pattern is that active power demand at each bus grows simultaneously according to the proportion of bus active power load at initial operating point, while load power factor keep constant, as expressed by (22) and (23).

$$P_{Li}(\lambda) = P_{Li0} \cdot (1+\lambda) \tag{22}$$

$$Q_{Li}(\lambda) = Q_{Li0} + \lambda \cdot K_{Li} \cdot P_{Li0} \tag{23}$$

where $P_{Li0}$ and $Q_{Li0}$ stand for base active and reactive load levels of bus $i$ in the initial operating state. $K_{Li}$ is a constant used to represent constant power factor load. Active power demand increment of the entire system is dispatched among conventional generators according to their base active power generation in the initial operating state, which can be written as

$$P_{Gi}(\lambda) = P_{Gi0} + \lambda \cdot P_{Gi0} \cdot \sum_{i=1}^{N} P_{Li0} \Big/ \sum_{i=1}^{N} P_{Gi0} \tag{24}$$

where $P_{Gi0}$ stands for base active power generation of bus $i$ in the initial operating state.

**Table 1.** IEC IIA wind turbine parameters

| $P_r$ (MW) | $v_{ci}$ (m/s) | $v_r$ (m/s) | $v_{co}$ (m/s) | cos $\theta$ |
|---|---|---|---|---|
| 2 | 2.5 | 13 | 25 | 0.90 |

## 6.2 Impact of wind speed correlation on *VSM*

In order to investigate the impact of correlated wind speeds on *VSM*, Monte Carlo simulation is implemented and *VSM* probability distribution under different correlation degree is obtained. Figs. 3 (a)~(c) illustrate *VSM* statistical histograms of the IEEE 57-bus system under wind speed correlation coefficients $\rho_{V4,5}$= $\rho_{V5,4}$= $\rho_{V54,55}$= $\rho_{V55,54}$= 0.1, 0.5 and 0.9 (abbreviated $\rho$, the same as follows) respectively, where the vertical axis $p$ denotes probability related with the corresponding horizontal axis *VSM* value. As shown in Fig. 3, the increase of wind speed correlation degree strengthens synchronization in power output of adjacent wind farms, thus active power generation as well as reactive power consumption of the wind farms with close locations increase and decrease simultaneously. These properties result in more fluctuation of the total wind

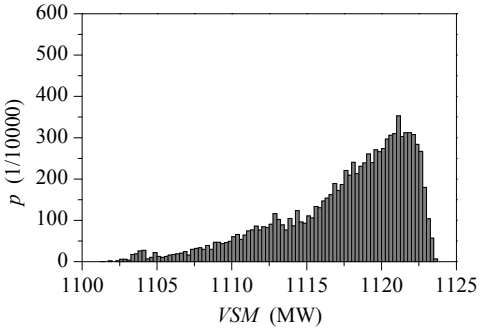


(a) $\rho$= 0.1

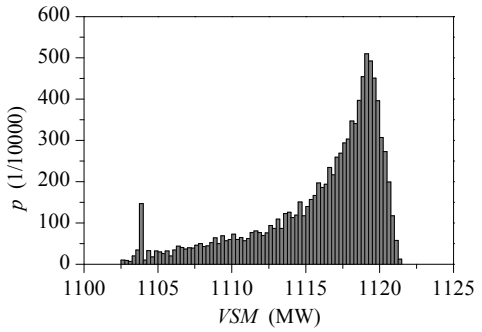


(b) $\rho$= 0.5

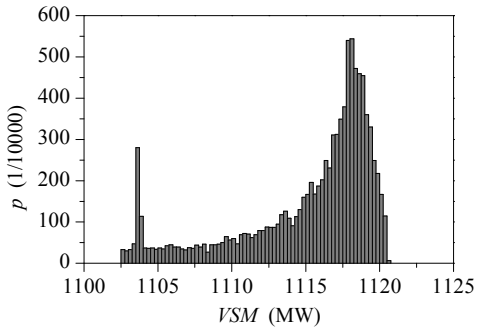


(c) $\rho$= 0.9

**Fig. 3.** Statistical histograms of *VSM* under different wind speed correlation coefficients

power output and consequently the probabilities of low and high distribution intervals of *VSM* are significantly larger.

The low value distribution of *VSM* in Fig. 3 means that voltage stability margin is inadequate, which is harmful to safe and stable operation of the power system. As a further analysis, the situations of $\rho$= 0.1~0.9 are also investigated. For each $\rho$, denote *VSM* value in the lowest 10% section of the entire *VSM* distribution range as Event-A, Table 2 lists *P*(Event-A), i.e. the occurrence probability of Event-A under different wind correlation coefficients. Based on the data summarized in Table 2, summing-ups similar with Fig. 3 can be easily achieved. With strengthening of WSC of adjacent wind farms, the probability of SNB appearances (i.e. voltage collapse) under relative lower load growth level increases. The presence of correlated wind speeds poses a potential threat to voltage stability, which should be taken seriously in power system planning and operation. Necessary precautions should be devised to avoid voltage stability deterioration caused by strong WSC.

**Table 2.** Occurrence probability of Event-A under different wind correlation coefficients

| $\rho$ | 0.1 | 0.2 | 0.3 | 0.4 | 0.5 | 0.6 | 0.7 | 0.8 | 0.9 |
|---|---|---|---|---|---|---|---|---|---|
| P(Event-A) (%) | 0.57 | 1.67 | 1.79 | 2.15 | 2.59 | 3.22 | 3.97 | 5.28 | 6.03 |

### 6.3 Impact of wind power penetration level on *VSM*

The case study in section 6.2 illustrates influence of correlated wind speeds on *VSM* probability distribution under condition of total 256 MW wind power. Here the impact of wind power penetration level is investigated by increasing total installation capacity of the four grid-connected wind farms to 384 MW and 512 MW, which are respectively 30% and 40% of active power load in the initial operating state of IEEE 57-bus system.

For weak, medium and strong WSC, i.e. $\rho$= 0.1, 0.5 and 0.9, probability distributions of *VSM* under different wind power penetration level are calculated. As the statistical indices summarized in Table 3, when $\rho$ being equal, with the growth of wind power installation capacity, the mean value of *VSM* probability distribution decreases, on the contrary, the standard deviation increases. Based on these results, it can be concluded that the augmentation of grid-connected wind power generation, as a whole, takes certain negative effect on voltage stability margin, the average value is reduced while the fluctuation is enhanced.

**Table 3.** Statistical indices of *VSM* under different wind power penetration level

| $\rho$ | Wind power penetration (%) | Mean value (MW) | Standard deviation (MW) |
|---|---|---|---|
| 0.1 | 20 | 1117.5538 | 4.3942 |
| | 30 | 1111.0509 | 10.2024 |
| | 40 | 1103.7425 | 15.1105 |
| 0.5 | 20 | 1115.9719 | 4.2829 |
| | 30 | 1111.6495 | 10.4858 |
| | 40 | 1102.6045 | 20.0199 |
| 0.9 | 20 | 1115.1646 | 4.6109 |
| | 30 | 1110.6098 | 10.8808 |
| | 40 | 1102.4714 | 21.4453 |

### 6.4 Impact of wind turbine's power factor on *VSM*

In this paper, it is assumed that all wind farms are equipped with the IEC IIA wind turbine. Main parameters of this type of wind turbine are listed in Table 1. Specially, the power factor is 0.90. Here the impact of wind turbine's power factor is investigated by modifying this factor to 0.85 and 0.95, while other parameters remain same as the case study in section 6.2.

For $\rho$= 0.1, 0.5 and 0.9, probability distributions of *VSM* under different wind turbine's power factor are calculated. As the statistical indices shown in Table 4, when $\rho$ is fixed, the increase of wind turbine's power factor results in greater mean value of *VSM* probability distribution, while the standard deviation decreases. The high value of power factor means that less reactive power consumption corresponding to a certain active power generation for a wind farm. This property implies some reactive power demand saving as the network reactive power loss and reactive power load increase, which is beneficial to the voltage stability.

**Table 4.** Statistical indices of *VSM* under different wind turbine's power factor

| $\rho$ | Power factor | Mean value (MW) | Standard deviation (MW) |
|---|---|---|---|
| 0.1 | 0.85 | 1112.8020 | 5.2673 |
| | 0.90 | 1117.5538 | 4.3942 |
| | 0.95 | 1118.2247 | 1.7739 |
| 0.5 | 0.85 | 1113.8472 | 6.1842 |
| | 0.90 | 1115.9719 | 4.2829 |
| | 0.95 | 1119.2437 | 2.7003 |
| 0.9 | 0.85 | 1112.4574 | 6.4595 |
| | 0.90 | 1115.1646 | 4.6109 |
| | 0.95 | 1117.8736 | 2.6860 |

### 6.5 Risk analysis application

The analysis in the previous section concentrates on *VSM* probability distribution under different correlation coefficients, here risk indexes defined in section 5 is adopted and risk analysis application is investigated. Fig. 4 illustrates the values of $Risk_1$ computed by (19) for correlation coefficients $\rho$=0.1, 0.5 and 0.9 versus *VSM*. As shown in Fig. 4, risk value corresponding to a specific *VSM* level increases when the correlation degree of adjacent wind farms increases. Take $VSM_S$=1115 MW as an instance, for $\rho$=0.1, 0.5 and 0.9, risks of voltage stability margin not achieving this given value are 24.41%, 30.26% and 33.34% respectively. Considering the amount of voltage stability margin deficiency, $Risk_2$ expressed by (20) is also studied and similar simulation result is demonstrated

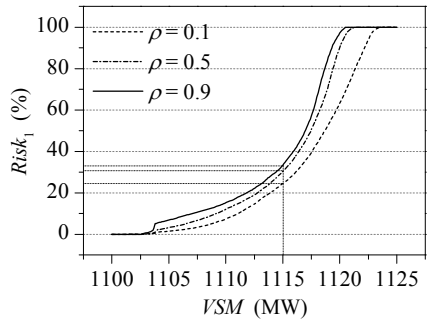


**Fig. 4.** $Risk_1$ ($VSM_S$) under different wind correlation coefficients

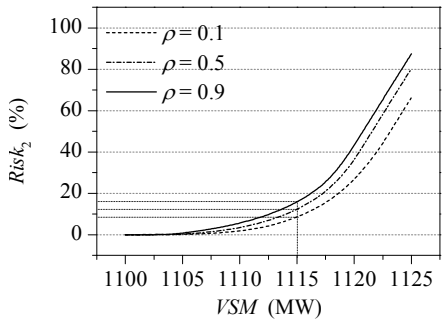


**Fig. 5.** $Risk_2$ ($VSM_S$) under different wind correlation coefficients

in Fig. 5. For $\rho$=0.1, 0.5 and 0.9, if the specific level $VSM_S$ is set as 1115 MW, risk of voltage stability margin shortage are respectively 8.59%, 12.31% and 15.83%.

From foregoing analysis, it is clear that the stronger the WSC of adjacent wind farms is, the greater the risk of voltage collapse for a given load growth level is, similarly the larger the amount of voltage stability margin deficiency is. More attention should be paid to correlated wind speeds in voltage stability research. Robust and efficient corrective measures for voltage stability margin improvement under strong WSC are worth further study. On the other hand, application of the presented risk indexes provides a more comprehensive analytical tool for voltage stability evaluation, which is proved to be one of the potentially useful techniques in practical power system with large-scale wind power penetration and strong wind speed correlation.

## 7. Conclusion

Impact of correlated wind speeds on power system voltage stability is comprehensively investigated in this paper. Strong WSC of adjacent wind farms leads to great probability of voltage collapse under relative lower load growth level, implying that the presence of correlated wind speeds is harmful to safe and stable operation of power system as far as voltage stability is concerned. Besides, impact of wind power penetration level and wind turbine's power factor on *VSM* are also investigated. Furthermore, two risk indexes are presented and the possible threat caused by WSC is evaluated from the viewpoint of risk analysis. The achievement of this paper gives a detailed elaboration about the influence of correlated wind speeds on voltage stability and provides a potentially effective analytical procedure for modern power system with wind power and other renewable energy power sources integration.

## Acknowledgements

This work was supported by the National Basic Research Program of China (973 Program) (2009CB219701) and the National Natural Science Foundation of China (50937002).

## References

[1] Van Cutsem T., "Voltage instability: phenomena, countermeasures, and analysis methods," *Proceedings of the IEEE*, Vol. 88, No. 2, pp. 208-227, Feb. 2000.

[2] Hossain M. J., Pota H. R., Mahmud M. A. and Ramos R. A., "Investigation of the Impacts of Large-Scale Wind Power Penetration on the Angle and Voltage Stability of Power Systems," *Systems Journal, IEEE*, Vol. 6, No. 1, pp. 76-84, March 2012.

[3] Ma Lei, Luan Shiyan, Jiang Chuanwen, Liu Hongling and Zhang Yan, "A review on the forecasting of wind speed and generated power," *Renewable and Sustainable Energy Reviews*, Vol. 13, No. 4, pp. 915-927, May 2009.

[4] Lim Jung-Uk and Jiang John N, "Bibliography review on applications of correlation analysis in power system operation and planning," *European Transactions on Electrical Power*, Vol. 20, No. 2, pp. 114-122, Mar. 2010.

[5] Morales J. M., Baringo L., Conejo A. J., and Minguez R., "Probabilistic power flow with correlated wind sources," *IET Generation, Transmission Distribution*, Vol. 4, No. 5, pp. 641-651, May 2010.

[6] Aien M., Fotuhi-Firuzabad M. and Aminifar F., "Probabilistic Load Flow in Correlated Uncertain Environment Using Unscented Transformation," *IEEE Transactions on Power Systems*, Vol. 27, No. 4, pp. 2233-2241, Nov. 2012.

[7] Chen Y., Wen J. and Cheng S., "Probabilistic Load Flow Method Based on Nataf Transformation and Latin Hypercube Sampling," *IEEE Transactions on Sustainable Energy*, Vol. 4, No. 2, pp. 294-301, Apr. 2013.

[8] Usaola J., "Probabilistic load flow with correlated wind power injections," *Electric Power Systems*

*Research*, Vol. 80, No. 5, pp. 528-536, May 2010.

[9] Qin Z., Li W. and Xiong X., "Generation System Reliability Evaluation Incorporating Correlations of Wind Speeds With Different Distributions," *IEEE Transactions on Power Systems*, Vol. 28, No. 1, pp. 551-558, Feb. 2013.

[10] Shu Z. and Jirutitijaroen P., "Latin Hypercube Sampling Techniques for Power Systems Reliability Analysis With Renewable Energy Sources," *IEEE Transactions on Power Systems*, Vol. 26, No. 4, pp. 2066-2073, Nov. 2011.

[11] Wu Liang, Park Jeongje, Choi Jaeseok and El-Keib A. A., "Probabilistic Reliability Evaluation of Power Systems Including Wind Turbine Generators Considering Wind Speed Correlation," *Journal of Electrical Engineering & Technology*, Vol. 4, No. 4, pp. 485-491, Dec. 2009.

[12] Billinton Roy, Gao Yi, and Karki Rajesh, "Composite System Adequacy Assessment Incorporating Large-Scale Wind Energy Conversion Systems Considering Wind Speed Correlation," *IEEE Transactions on Power Systems*, Vol. 24, No. 3, pp. 1375-1382, Aug. 2009.

[13] Gao Yi and Billinton Roy, "Adequacy assessment of generating systems containing wind power considering wind speed correlation," Renewable Power Generation, *IET*, Vol. 3, No. 2, pp. 217-226, June 2009.

[14] Bu S. Q., Du W., Wang H. F., Chen Z., Xiao L. Y. and Li H. F., "Probabilistic Analysis of Small-Signal Stability of Large-Scale Power Systems as Affected by Penetration of Wind Generation," *IEEE Transactions on Power Systems*, Vol. 27, No. 2, pp. 762-770, May 2012.

[15] Villanueva D., Feijoo A., and Pazos J. L., "Simulation of Correlated Wind Speed Data for Economic Dispatch Evaluation," *IEEE Transactions on Sustainable Energy*, Vol. 3, No. 1, pp. 142-149, Jan. 2012.

[16] Ditlevsen O. and Madsen H. O., Structural Reliability Methods: Wiley, 1996, p.115-116.

[17] Morales Juan M., Conejo Antonio J., and Perez-Ruiz Juan, "Simulating the Impact of Wind Production on Locational Marginal Prices," *IEEE Transactions on Power Systems*, Vol. 26, No. 2, pp. 820-828, May 2011.

[18] Sudati Sagrilo Luis Volnei, Prates de Lima Edison Castro, and Papaleo Arnaldo, "A Joint Probability Model for Environmental Parameters," *Journal of Offshore Mechanics and Arctic Engineering*, Vol. 133, No. 3, article ID 031605, Aug. 2011.

[19] Liu Pei-Ling and Der Kiureghian A., "Multivariate distribution models with prescribed marginals and covariances," *Probabilistic Engineering Mechanics*, Vol. 1, No. 2, pp. 105-112, June 1986.

[20] Li HongShuang, Lue ZhenZhou and Yuan XiuKai, "Nataf transformation based point estimate method," *Chinese Science Bulletin*, Vol. 53, No. 17, pp. 2586-2592, Sep. 2008.

[21] Safari Bonfils and Gasore Jimmy, "A statistical investigation of wind characteristics and wind energy potential based on the Weibull and Rayleigh models in Rwanda," *Renewable Energy*, Vol. 35, No. 12, pp. 2874-2880, Dec. 2010.

[22] Morgan Eugene C., Lackner Matthew, Vogel Richard M., and Baise Laurie G., "Probability distributions for offshore wind speeds," *Energy Conversion and Management*, Vol. 52, No. 1, pp. 15-26, Jan. 2011.

[23] Hetzer John, Yu David C., and Bhattarai Kalu, "An Economic Dispatch Model Incorporating Wind Power," *IEEE Transactions on Energy Conversion*, Vol. 23, No. 2, pp. 603-611, June 2008.

[24] Available online: http://www.vestas.com/en/wind-power-plants/procurement/turbine-overview/v90-1.8/2.0-mw.aspx#/vestas-univers.

[25] Tsili M. and Papathanassiou S., "A review of grid code technical requirements for wind farms," *IET Renewable Power Generation*, Vol. 3, No. 3, pp. 308-332, Sep. 2009.

[26] V. Ajjarapu and C. Christy, "The continuation power flow: A tool for steady state voltage stability analysis," IEEE Transactions on Power Systems, Vol. 7, No. 1, pp. 416-423, Feb. 1992.

[27] Cao G. Y. and Hill. D. J., "Power system voltage small-disturbance stability studies based on the power flow equation," *IET Generation, Transmission Distribution*, Vol. 4, No. 7, pp. 873-882, July 2010.

[28] Avalos Rafael J., Canizares Claudio A., Milano Federico and Conejo Antonio J., "Equivalency of Continuation and Optimization Methods to Determine Saddle-Node and Limit-Induced Bifurcations in Power Systems," *IEEE Transactions on Circuits and Systems I: Regular Papers*, Vol. 56, No. 1, pp. 210-223, Jan. 2009.

[29] Cañizares Claudio A., "Conditions for saddle-node bifurcations in AC/DC power systems," *International Journal of Electrical Power & Energy Systems*, Vol. 17, No. 1, pp. 61-68, Feb. 1995.

[30] Jiang Wei, Wang Chengshan, Yu Yixin and Zhang Pei, "A New Method for Direct Calculating the Critical Point of Static Voltage Stability," *Proceedings of the CSEE*, Vol. 26, No. 10, pp. 1-6, Mar. 2006. (in Chinese)

[31] Falaghi Hamid, Ramezani Maryam, Singh Chanan, and Haghifam Mahmood-Reza, "Probabilistic Assessment of TTC in Power Systems Including Wind Power Generation," *IEEE Systems Journal*, Vol. 6, No. 1, pp. 181-190, Mar. 2012.

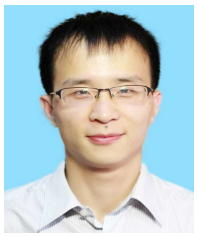

**Hongxin Li** He received the B.Eng. degree in electrical engineering from Huazhong University of Science and Technology (HUST), Wuhan, China in 2007, where he is currently pursuing the Ph.D. degree. His research interests include voltage stability, reactive power optimization and control, and renewable energy.

**DeFu Cai** He received the B.Eng. degree in electrical engineering from Huazhong University of Science and Technology (HUST), Wuhan, China in 2009, where he is currently pursuing the Ph.D. degree. His research interests include renewable energy, micro-grid, electric vehicle and power system analysis.

**Yinhong Li** She received the B. Eng. degree and the Ph.D. degree in electrical engineering from Huazhong University of Science and Technology (HUST), Wuhan, China in 1998 and 2004, respectively. Dr. Li is an associate professor in the College of Electrical and Electronic Engineering at HUST. Her research interests include relay coordination, voltage stability, and load modeling.